optica

Photoconductive heaters enable control of large-scale silicon photonic ring resonator circuits: supplementary material

HASITHA JAYATILLEKA[1,2,3,*], HOSSAM SHOMAN[1,3,*], LUKAS CHROSTOWSKI[1], AND SUDIP SHEKHAR[1]

[1]Department of Electrical and Computer Engineering, University of British Columbia, 2332 Main Mall, Vancouver, British Columbia V6T 1Z4, Canada

[2]Currently with Intel Corporation, 2200 Mission College Blvd, Santa Clara, California, 95054, USA

[3]Contributed equally to this work

[*]Corresponding author: hasitha@ece.ubc.ca, hoshoman@ece.ubc.ca

Published 15 January 2019

This document provides supplementary information to "Photoconductive heaters enable control of large-scale silicon photonic ring resonator circuits," https://doi.org/10.1364/OPTICA.6.000084. Details are provided about fabrication, design, and experimental procedures for the devices presented in the main article.

1. DEVICE DESIGN AND FABRICATION

The silicon rib nanowire waveguides were designed to be 500 nm-wide and 220 nm-high, with 90 nm-thick slab sections to the sides of the waveguide core (see Fig. 1 of paper). Photoconductive heaters were created by n-doping the center of the waveguides (5×10^{17} cm^{-3}). The slab sections of the waveguides 500 nm away from the core were heavily doped to form ohmic contacts to the silicon. Fig. S2c shows a measured IV curve of 100 µm long photoconductive heater. The resistance of the device at 1 V is 1.3 kΩ.

The switch's ring resonators were designed to have a radius of 8 µm. The bus-to-ring gaps were chosen to be 200 nm for all of the rings. The photoconductive heater occupied 25% of the microring's circumference (12.55 µm). The ground connections of all 256 photoconductive heaters were connected together. The input and cross-ports of the switch corresponding to several selected routes were connected to grating couplers to facilitate optical inputs and outputs. The switch's ring resonators were arranged in a square grid with a spacing of 150 µm between the adjacent rings. The spacing can be further reduced by decreasing the footprint of the contact pads. Reducing the spacing between the rings can increase the amount of thermal crosstalk. We measured the detuning of a ring due to crosstalk heating from a ring located 100 µm away to be about 2.5 pm/mW dissipated by the aggressor (only two rings were activated with the victim and aggressors dissipating 5 mW and 20 mW, respectively).

In the CROW, circumference of each ring was 66.83 µm with a circular section of radius 10 µm and a straight coupling section of 2 µm. The coupling gaps between the bus-waveguides and the rings were chosen to be 200, 400, 475, 510, 520, 526, 528, 530, 528, 526, 520, 510, 475, 400, and 200 nm for a flat-top passband transmission and a wide bandwidth. Fig. S1 shows the simulated response of the filter. The coupling between waveguides was simulated using the finite difference time domain (FDTD) method. The overall response was then computed using the transfer matrix method. In each ring, the photoconductive heater occupied 10.47 µm waveguide section. The doped sections were defined to be on the opposite sides of the adjacent rings in order to minimize the electrical crosstalk between their heaters. The entire device, including the contact pads and metal routing and pads occupied an area of 1480 µm×280 µm. Grating couplers were used for optical inputs/outputs.

All of the devices were fabricated using 248 nm deep UV lithography in a silicon photonics processing line through Institute of Microelectronics (IME), A*STAR, Singapore[1]. All the doping layers (n and n^{++}) used in this work are standard to this processing line.

2. PHOTOCONDUCTIVITY MEASUREMENTS

The QE of the photoconductive heater can be calculated from,

$$\mathrm{QE} = \frac{I_{\mathrm{PD}}/q}{P_{\mathrm{absorbed}}/h\nu}, \tag{S1}$$

where q is the electron charge, h the Planck's constant and ν the optical frequency. Optical power absorbed, P_{absorbed}, was calculated as $P_{\mathrm{absorbed}} = P_0(1 - e^{-\alpha l})$, where P_0 is the optical power

(in linear scale) going into the device, α the propagation losses in photoconductive heater in cm^{-1}, and l the length of the doped waveguide in centimeters. P_0 was calculated by measuring the response of loopback structure with grating couplers at 1.55 µm wavelength, P_{GC} (in dB). If the laser's input power is P_{in} (in dBm) then $P_0 = P_{in} - P_{GC}/2$ (in dBm). The propagation loss of the doped waveguide sections (α) was measured by fitting the spectra of a similarly doped microring's response[2], where the doping losses were extracted to be about 5 dB/cm. The photoconductive heater's photodetection bandwidth was measured using the setup shown in Fig.S4b. The CW laser was internally modulated at 500 kHz generating a square signal with 50% duty cycle. A bias-T was used to bias the photoconductive heater and pass the AC photocurrent signal to an oscilloscope to display the temporal response of the photoconductive heater.

3. ELECTRO-OPTICAL SETUP FOR SWITCH AND CROW

The fabricated chips were assembled in an 84-pin Kyocera ceramic quad flat non-leaded chip carriers (PB-C86131). The devices were connected to the chip carriers via wirebonds. The chip carriers were placed in an 84-pin socket (AE11110-ND) and soldered to an FR-4 PCB. This PCB was placed on a 6-axis controlled stage, and connected to a source-measure circuit via jumper wires for electrical I/O. A fiber array with single mode polarization maintaining fibers was used to couple light into and out of the chip (See Fig.S3). Our source-measure circuit consisted of a 2 channel Keithley 2602 source measure unit (SMU), 64 voltage sources (by combining NI PXI-6704 and NI PXIe-6738), 2 Arduino Mega 2560 microcontrollers and in-house designed electrical switch board using MAX4053ACPE+ switch chips. The switchboard facilitated connecting either of the SMU channels or the voltage sources to the ring heaters as required. The Arduino boards supplied the digital logic to the switch board. A personal computer was used for controlling the SMU, voltage sources, and the switch board via the Arduinos. In the experiments presented in sections 3 and 4 of the paper, the output tuning voltages supplied to the rings were limited to a range of 0.1 V - 6.0 V. Fig.S4 shows a block diagram of this arrangement. We used a Keysight N7714A as the input light source for tuning. An Agilent 81682A tunable laser and a Keysight N7744A photodetector or an optical vector analyzer (Luna OVA 5000) were used to obtain the optical sweeps after tuning the 16×16 switch and the 14-ring CROW.

REFERENCES

1. "Fab: Advanced micro foundry (AMF) silicon photonics fabrication process," https://www.cmc.ca/en/WhatWeOffer/Products/CMC-00200-03001.aspx. Accessed: 2018-6-22.
2. M. Popović, *Theory and Design of High-index-contrast Microphotonic Circuits* (2008).

4. SUPPLEMENTARY FIGURES

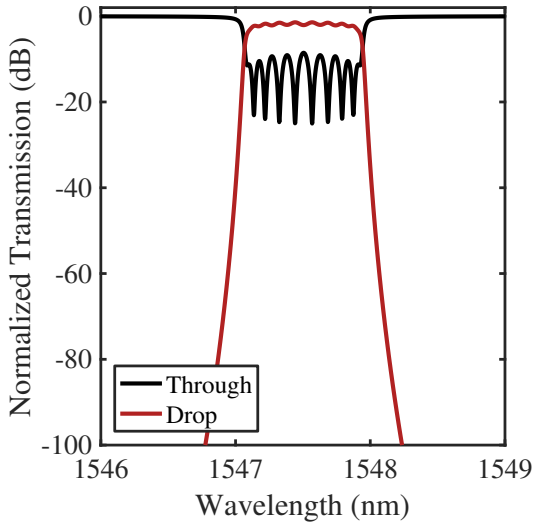

Fig. S1. Simulated response of the 14-Ring CROW as described in section S1. We attribute the mismatches between simulated and post-tuned response shown in Fig. 7c of the paper mainly to variation of the coupling gaps in fabrication. As the coupling sections are not tunable in this design, the deviations due to variations in coupling cannot be corrected post-fabrication by thermo-optic tuning.

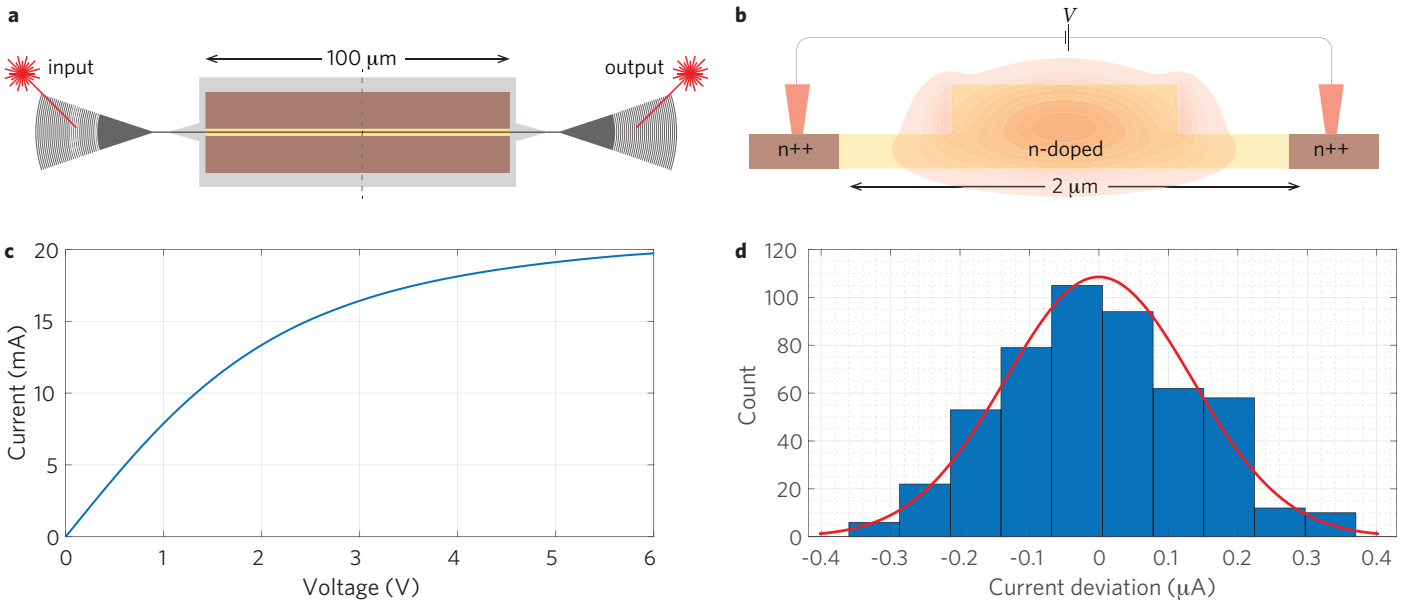

Fig. S2. Photoconductive heater used for QE measurements. (a) Layout top-view of the photoconductive heater used in the QE measurements. (b) Cross-section of the photoconductive heater. (c) Dark current of the photoconductive heater across the voltage applied to the heater's terminals. (d) 500 measurements of the dark current taken over 4 minutes. The standard deviation (σ) is 0.15 µs.

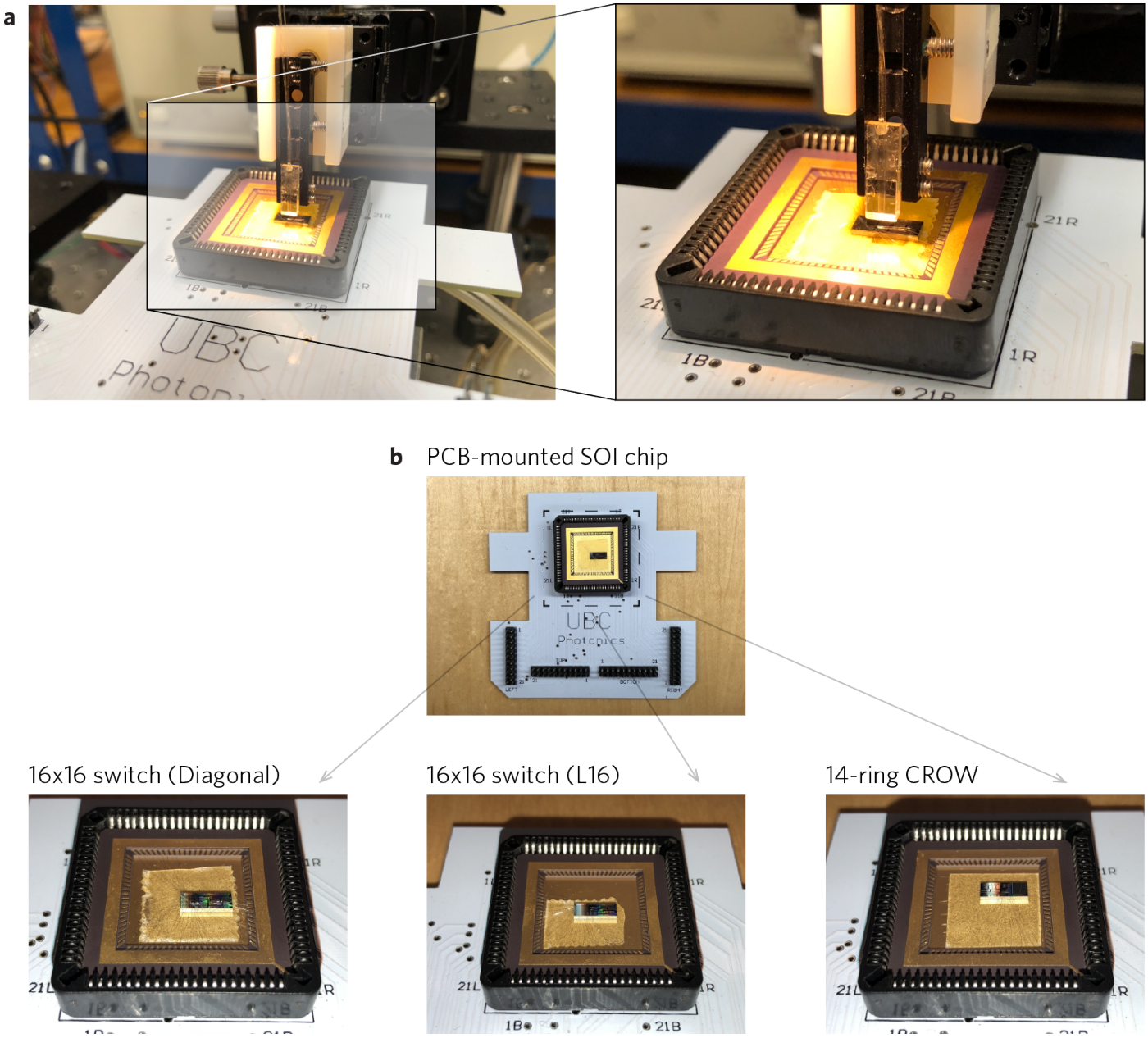

Fig. S3. Chip packaging for optical testing. (a) A fiber array with single mode polarization maintaining fibers was used to couple light into and out of the chips. The inset shows a zoomed-in view of the fiber array. The PCB shown is placed on a 6-axis controlled stage. (b) Top view of the fabricated chip assembled in an 84-pin Kyocera ceramic quad flat non-leaded chip carriers, placed in an 84-pin socket and soldered to an FR-4 PCB. The devices were connected to the chip carriers via wirebonds. The inset shows a close-up view of the wirebonded chips for each of the devices demonstrated in the paper: 1) the 16x16 switch for the diagonal case, 2) 16x16 switch for the L16 case, and 3) the 14-ring CROW.

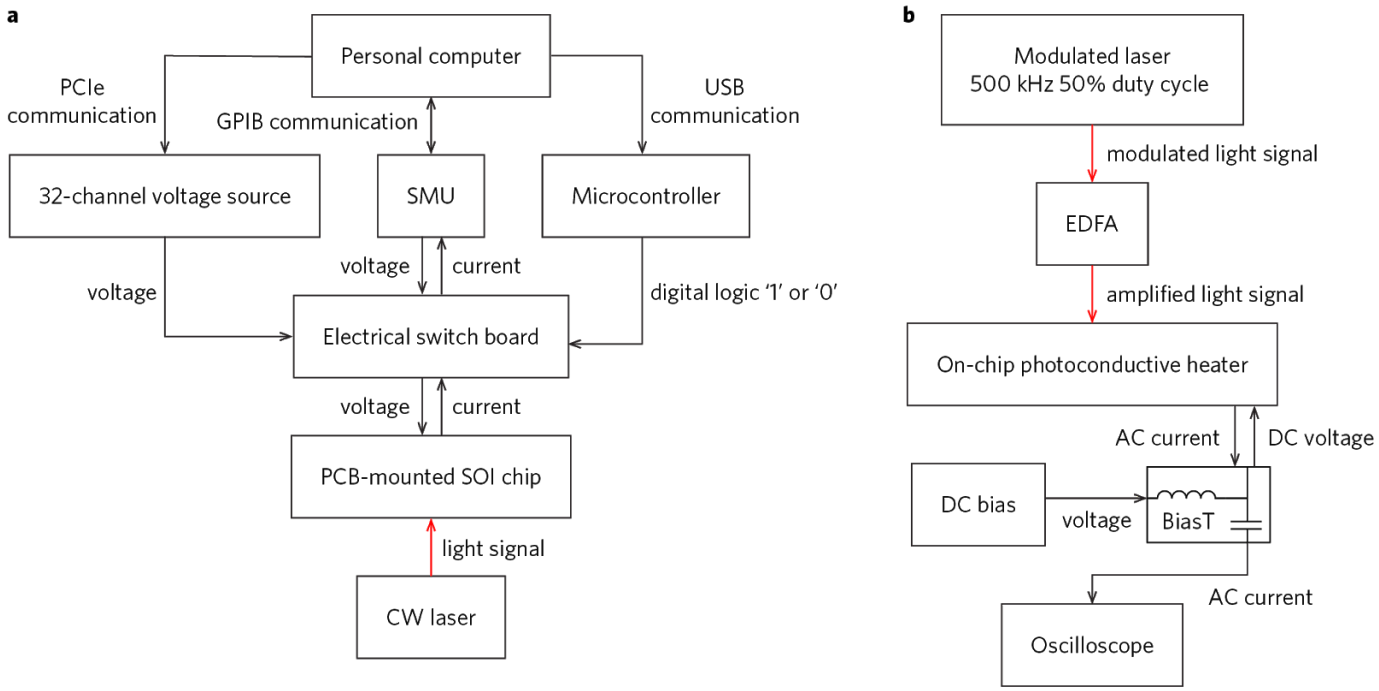

Fig. S4. Optical and electrical test setup configurations. (a) The block diagram of the setup used for tuning the 16x16 switch and the 14-ring CROW. The black and red lines lines indicate the electrical and optical signals, respectively. (b) The block diagram of the setup used to measure the temporal response of the photoconductive heater.

Table 1: Switch losses breakdown.

Path	Crossings	Rings	Total loss (dB)
$L_1 : I_1 \rightarrow C_1$	15	1	~ 8
$L_{16} : I_1 \rightarrow C_16$	30	1	~ 14
Diagonal : $I_1 \rightarrow C_{16}$	30	31	~ 21.5

Fig. S5. Breakdown of the measured losses in each path of the switch.

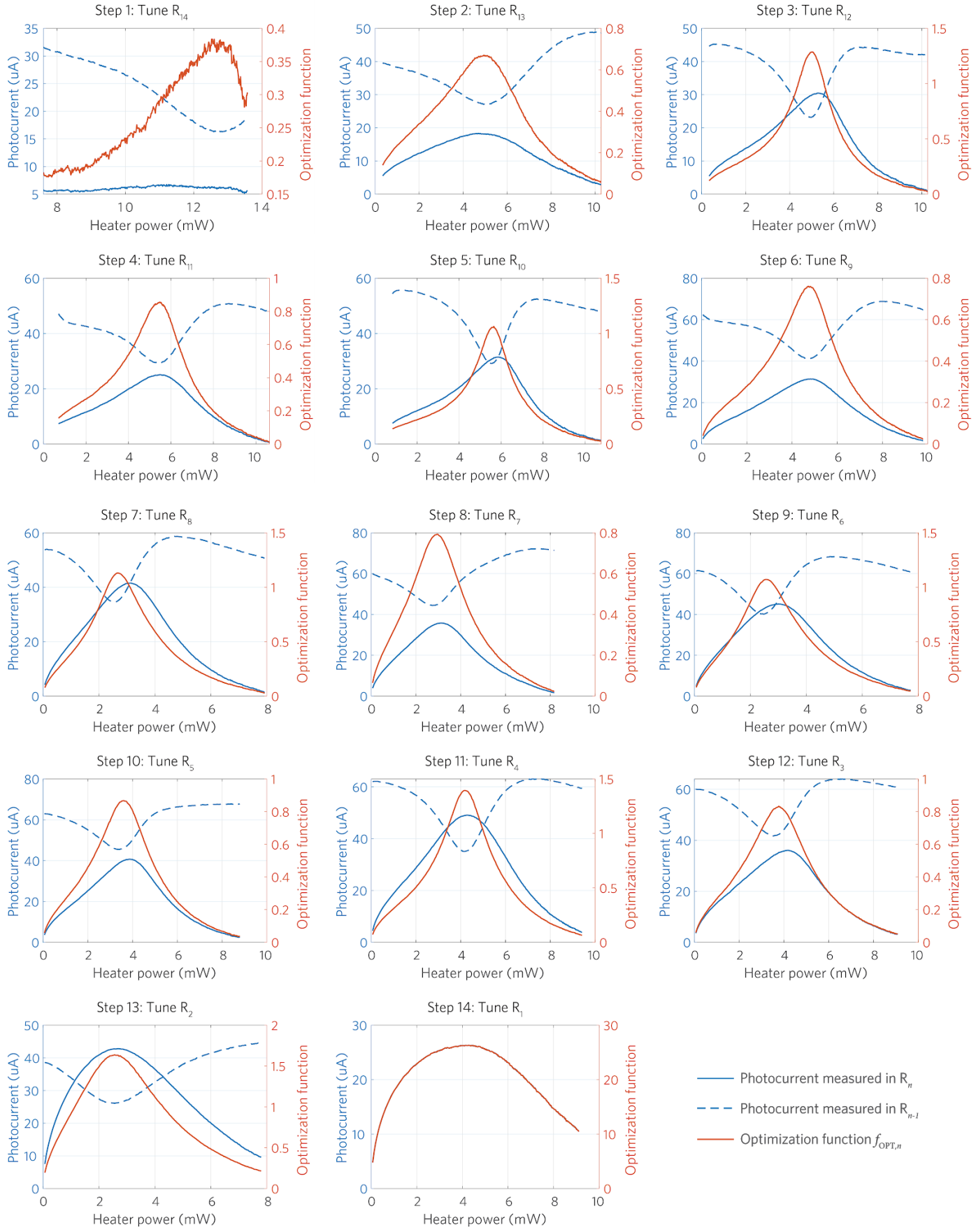

Fig. S6. Measured photocurrents and the optimization functions corresponding to each of the steps when tuning the 14-ring CROW. The rings R_{14}, which is coupled to the drop-port, through R1, which is coupled to the through-port, were tuned. The optimization functions shown in the figures were calculated as $I_{PD,n}/I_{PD,n-1}$, where $I_{PD,n}$ is the photocurrent measured in the nth ring. For the last ring tuned, R_1, the optimization function was it's photocurrent $I_{PD,1}$. After each step, the voltages of the tuned ring R_n, was set to the voltage that maximed the optimization function.